Sublimation's impact on temporal change of albedo dichotomy on Iapetus

Jun Kimura [a,b] Taichi Kawamura [c] Hisataka Morito [c] Tomokatsu Morota [d] Chikatoshi Honda [e] Kiyoshi Kuramoto [a,b] Tatsuaki Okada [d]

[a] *Department of Cosmosciences, Hokkaido University, Nishi-8 Kita-10, Kita-Ku, Sapporo 060-0810, Japan*

[b] *Center for Planetary Science, Kobe University, Nada-ku Rokkodai-cho 1-1, Kobe 657-8501, Japan*

[c] *The University of Tokyo, 7-3-1 Hongo, Bunkyo-Ku, Tokyo 113-0033, Japan*

[d] *RISE Project, National Astronomical Observatory of Japan, 2-21-1 Osawa, Mitaka 181-8588, Japan*

[e] *The University of Aizu, Ikki-machi, Aizu-wakamatsu, Fukushima 965-8580, Japan*

Abstract

Iapetus, one of the Saturnian moons, has an extreme albedo contrast between the leading and trailing hemispheres. The origin of this albedo dichotomy has led to several hypotheses, however it remains controversial. To clarify the origin of the dichotomy, the key approach is to investigate the detailed distribution of the dark material. Recent studies of impact craters and surface temperature from Cassini spacecraft data implied that sublimation of H_2O ice can occur on Iapetus' surface. This ice sublimation can change the albedo distribution on the moon with time.

In this study, we evaluate the effect of ice sublimation and simulate the temporal change of surface albedo. We assume the dark material and the bright ice on the surface to be uniformly mixed with a certain volume fraction, and the initial albedo distribution to incorporate the dark material deposits on the surface. That is, the albedo at the apex is lowest and concentrically increases in a sinusoidal pattern. This situation simulates that dark materials existed around the Iapetus' orbit billions of years ago, and the synchronously rotating Iapetus swept the material and then deposited it on its surface. The evolution of the surface albedo during 4.0 Gyr is simulated by estimating the surface temperature from the insolation energy on Iapetus including the effect of Saturn's eccentricity and Iapetus' obliquity precession, and evaluating the sublimation rate of H_2O ice from the Iapetus' surface.

As a result, we found that the distribution of the surface albedo changed dramatically after 4.0 Gyr of evolution. The sublimation has three important effects on the resultant surface albedo. First, the albedo in the leading hemisphere has significantly decreased to approach the minimum value. Second, the albedo distribution has been elongated along the equator. Third, the edge of the low albedo region has become clear. Considering the effect of ice sublimation, the current albedo distribution can be reconstructed from the sinusoidal albedo distribution, suggesting the apex–antapex cratering asymmetry as a candidate for the origin of the albedo dichotomy. From the model analysis, we obtained an important aspect that the depth of the turn–over layer where the darkening process proceeded for 4 Gyr should be an order of 10 cm, which is consistent with evaluation from the Cassini radar observations.

Key words: Iapetus, Saturn, satellites, Satellites, surfaces, Ices, Geological processes

1 Introduction

Iapetus, Saturn's third–largest moon, has a diameter of approximately 1436 km and synchronously orbits Saturn at an average distance of 3.6×10^6 km with a period of 79.3 Earth days. From

the mean density of 1080 kg/m^3 and the spectral observations from spacecrafts and ground telescopes (Table 1), it is implied that Iapetus has a large volume fraction of H_2O ice.

One of the remarkable characteristics of Iapetus is an albedo dichotomy between the leading and trailing hemispheres by an order of magnitude; visible reflectances of the leading and trailing hemispheres are about 5 % and 60 %, respectively (e.g., Hendrix and Hansen (2008)), thus resembling a Yin-Yang symbol (Fig. 1). The enigmatic dark region, covering the leading hemisphere, is called the Cassini Regio. The dichotomy is generally considered to originate from the dark material different from H_2O ice rather than from a difference of crystalline structure or a metamorphosis of H_2O ice (Jaumann et al., 2009).

The composition of the dark material is still unknown, however a mixture of tholin, carbon dioxide, aromatic hydrocarbons, and other non-water materials has been suggested as a candidate material from some experimental studies and spectral analyses (Veeder and Matson, 1980; Lebofsky et al., 1982; Smith et al., 1982; Squyres, 1983; Bell et al., 1985; Owen et al., 2001; Buratti et al., 2005; Filacchione et al., 2007; Cruikshank et al., 2008; Hendrix and Hansen, 2008).

Two major hypotheses of the origin of the albedo dichotomy on the Iapetus' surface have been proposed (Soter et al., 1974; Cruikshank et al., 1983; Buratti and Mosher, 1995; Vilas et al., 1996; Owen et al., 2001). One hypothesis suggests that the dark material may have originated from other satellites, i.e., the outer moon Phoebe, which has a very low albedo (e.g., Bell et al. (1985); Thomas and Veverka (1985); Verbiscer et al. (2009)). In this case, impacts ejected the dark materials from other satellites, then the materials traveled to the Iapetus' orbit, where Iapetus swept them. This is the so-called "external hypothesis" (Buratti et al., 2008), which is supported by the fact that the dark materials are concentrated on the leading hemisphere and do not depend on any specific morphology, for example, tectonic or impact features

implying volcanic or other endogenic activity (Fig. 2). Moreover, spectral characteristics of the dark material are partially similar to that of the material on Phoebe (e.g., Jarvis et al. (2000); Buratti et al. (2005); Filacchione et al. (2007)). Also, recent experimental works reported that the interplanetary material and the cometary dust have some similarities with the Iapetus' dark material (Cruikshank et al., 2008).

Another hypothesis presumes that the dark materials were ejected from a ridge and deposited on the surface. This is the so-called "endogenic hypothesis" (Smith et al., 1982; Denk et al., 2005), that is based on the fact of view that a topographic ridge on Iapetus coincides almost exactly with the geographic equator, which spreads over a length of ∼1600 km (Castillo-Rogez, 2007), and appears to be related to the distribution of the dark material.

Whether the ridge spreads to the bright region is uncertain because of the low resolution of the images captured from the Voyager and Cassini spacecraft. In addition, the energetics of the eruption of the dark material, which is denser than bright H_2O ice, is highly questionable (Denk and Neukum, 2000).

2 Ice sublimation and albedo change

The dark region on Iapetus is distributed with mainly two local and global characteristics. The distribution of the dark region on the Iapetus' craters has a geometric trend, i.e., the equator–facing wall and the floor of several craters at low and middle latitudes appear darker whereas the other side is bright. On the other hand, craters at higher latitudes do not show the dark region on any side of the wall or floor (Fig. 3). This trend can be interpreted as follows. Pure bright ice has sublimed from the equator-facing wall where the insolation energy is higher than that at other walls. Thus, the albedo of the equator-facing wall has decreased. The Cassini spacecraft observed the surface temperature by us-

ing the mid-infrared wavelength: the maximum temperature in the dark region during daytime was found to be approximately 130 K (Spencer and Denk, 2010). The saturated vapor pressure of H_2O ice at 130 K is approximately 1.2×10^{-10} Pa (Andreas, 2007). The effects of ice sublimation on the surface albedo and its morphology have been previously discussed for other icy satellites (Spencer, 1987).

Another characteristic of the albedo dichotomy is the clarity of the edges of the dark region. If the dark material was deposited on the surface from external sources, the distribution of the dark material should be more gradual than the current state. Therefore, the sublimation of bright ice and the resultant albedo change must affect the current distribution of the surface albedo on Iapetus. In other words, the volume fraction of the dark material and the ice in each region is expected to have changed with time, and the albedo distribution when the dark material was originally deposited is expected to be different from the current state.

Saturn has an orbital eccentricity of 0.056, which indicates that the distance to the Sun will change from 9.05 to 10.1 AU. This difference could considerably affect insolation throughout the Saturn year. In addition, Iapetus' obliquity (the inclination relative to Saturn's orbital plane) can periodically change between 4.3 degrees and 19.3 degrees with a 3000–year cycle, because the longitude of the Iapetus' ascending node precesses with a period of 3000 years as Iapetus maintains an almost constant obliquity of 7.5 degress relative to the Laplace plane (Ward, 1981; Sinclair, 1974; Palmer and Brown, 2008). This precession has a possibly significant effect on solar insolation.

In this study, we evaluate the effect of ice sublimation on the surface albedo of Iapetus and the temporal change, and attempt to reconstruct the pristine distribution of the dark material on Iapetus and to constrain the surface thickness and the origin of the dark materials. We do not consider the effect of a recondensation of the sublimed ice (see Section 5)

3 Methods

On the basis of the position of Iapetus in its orbit, the insolation energy on the Iapetus' surface can be calculated, and the radiative equilibrium temperature and its surface distribution can be estimated by the Stefan–Boltzmann's law. Iapetus rotates around Saturn with a period of approximately 79.3 Earth days, and its obliquity relative to the equatorial plane of Saturn is approximately 15.4 degrees (Sinclair, 1974).

For the surface structure on Iapetus, the incoming exogenic dark materials and the surface bright ice are initially assumed to have mixed uniformly with a certain fraction $f_0 = V_{ice0}/V$ down to a depth that is much greater than the turn–over depth d (Fig. 5). V is the total volume of the turn–over layer with unit surface area and V_{ice0} is that of H_2O ice initially included in this layer. This simulates that the dark material, which is originated from Phoebe and/or outside the Saturnian system, was traveled inward and deposited on ancient Iapetus. After some time, the bright ice is sublimated from the turned-over layer, and the current fraction in the turned-over layer is f, which is different from f_0. The surface Bond albedo can be calculated by linear mixing model as follows,

$$A = f A_{ice} + (1 - f) A_{dark}, \tag{1}$$

where $f = V_{ice}/V$, V_{ice} is the total volume of H_2O ice included in this layer. A_{ice} and A_{dark} are the albedos of the pure H_2O ice and the dark material, respectively. The use of a volume ratio to obtain the albedo of mixed material is only correct when materials are intimately mixed with each other

$$S_{ice} = S\frac{V_{ice}}{V} = S \cdot f, \tag{2}$$

where S is the surface area, and S_{ice} is that of the ice. Volume fraction model are frequently used to represent the optical properties of mixed constituents as most simplified way in the Earth

and planetary subjects (e.g., Cuzzi and Estrada. (1998); Ackerman (1981); Dozier and Warren. (1982)), however it may be useful to note that only the first few microns are the optically relevant for the Bond albedo.

Ice can be sublimed depending on the temperature. The radiative equilibrium temperature at the Iapetus' surface can be calculated as

$$\varepsilon\sigma T^4 = (1 - A)\, E \cdot \sin\phi, \tag{3}$$

where ε is the emissivity of the surface, σ is the Stefan–Boltzmann constant, T is the temperature, E is the solar radiation at the Saturn system, and ϕ is the solar altitude in degrees, with 0 degree being the horizon and 90 degrees the zenith (Fig. 4). For example, when the surface Bond albedo is 0.1, the radiative equilibrium temperature is 127.5 K, whereas when the Bond albedo is 0.04, the temperature is 129.6 K (with $\varepsilon = 0.9$ and $\phi = 90°$) The observed temperature acquired by Cassini spacecraft VIMS is approximately 129 K in the low albedo region at midday (Spencer and Denk, 2010). This indicates that the radiative equilibrium temperature defined by Eq. 3 agrees with the observation. It also agrees with the assumption that the surface is covered with regolith-like material of low thermal inertia, which is probably formed by the impact gardening process.

Using the surface condition for a given temperature, we evaluate the possibility of the sublimation of surface ice. On the basis of the experimental data about the saturated vapor pressure of H_2O ice (Andreas, 2007), we evaluate the sublimation rate of ice from the surface by using the following equation (e.g., Estermann (1955); Andreas (2007))

$$\dot{K}_{sub} = e(T) \left(\frac{M_w}{2\pi RT} \right)^{1/2}, \tag{4}$$

where $\dot{K}_{sub}$ is the mass rate of sublimation of pure H_2O ice per

unit area (kg/m^{2}s), $e(T)$ is the saturated vapor pressure of pure ice, M_W is the molar weight of H_2O, and R is the gas constant. Although experimental results of saturated vapor pressure in the lower temperature region (lower than 130 K) for the Iapetus' surface have not been acquired, the following relationship can be found by extrapolating the previous experimental results to the lower temperature (Murphy and Koop, 2005; Andreas, 2007)

$$e(T) = \exp\left(C_1 - \frac{C_2}{T} + C_3 \ln T - C_4\, T\right)[Pa], \tag{5}$$

where $C_1 = 9.550426$, $C_2 = 5723.265$, $C_3 = 3.53066$, and $C_4 = 0.0072833$.

Considering Eq.2, the temporal change of the mass of ice can be expressed as

$$\frac{dM_{ice}}{dt} = -\dot{K}_{sub} \cdot\ S_{ice} = -\dot{K}_{sub} S \frac{V_{ice}}{V} = -\dot{K}_{sub} S \cdot\ f, \tag{6}$$

where M_{ice} is the mass of pure ice, and t is the time. The loss of ice will reduce the albedo. We calculate the evolution of the surface albedo distribution over billions of years.

The layer loses $d\phi = dV/V$, which dV is the cumulative volume of sublimated ice, because of sublimation, and because the turn–over depth d and total volume V remain the same, the turned-over layer incorporates an equal amount of ungardened material from below (Fig. 5). This ungardened layer has f_0 fraction of ice and $1 - f_0$ fraction of dark material. Because we assume that the turn–over process does not add the dark material but rather just mixes the existing materials, the turn–over layer has lost $d\phi$ of ice because of sublimation, and has gained $d\phi \cdot\ f_0$ of ice because of incorporating ice from below for a net loss of $d\phi(1-f_0)$. Similarly, the gain of the dark material is $d\phi(1-f_0)$. Volumetric sublimation

rate is given by using Eq.6 as follows,

$$\frac{dV}{dt} = \frac{d\left(M_{ice}/\rho_{ice}\right)}{dt} = \frac{1}{\rho_{ice}}\frac{dM_{ice}}{dt} = -\frac{\dot{K}_{sub}S \cdot f}{\rho_{ice}}, \tag{7}$$

and finally,

$$\frac{d\phi}{dt} = \frac{dV/V}{dt} = \frac{1}{V}\frac{dV}{dt} = -\frac{\dot{K}_{sub}S \cdot f}{V\rho_{ice}}. \tag{8}$$

As for the time-steps, in order to calculate the long-term (for 4 Gyr) change of albedo we consider the time-step of 1000 years which is less than the period of Iapetus' obliquity change (3000 years). On the other hand, in the evaluation of the change of the solar elevation angle on Iapetus' surface we use the time-step of 1 Earth day which is sufficiently less than the Iapetus' orbital period (79.33 Earth days) using the Euler method for numerical integration with time as the independent variable. Even if finer time-steps are used, the whole results would not change. In a short time scale within dt, we assume that the sublimation should occur in the surface thin layer which has been well-mixed due to the impact gardening, and this thin layer corresponds to the mixing layer suggested by Gault et al. (1974). On the other hand, in a long timescale, larger impacts occurred at a certain probability can excavate (turn–over) to the deeper region (turn–over depth d) that corresponds to the depth of turn–over within 10^9 years shown in Gault et al. (1974).

The initial ice volume fraction in the turn–over layer was f_0, thus it will have no ice when

$$d\phi(1 - f_0) = dV(1 - f_0)/V = f_0, \tag{9}$$

which occurs when the amount $d\phi = f_0/(1 - f_0)$ has been lost, and it yields

$$dV(1 - f_0) = V \cdot f_0 = V_{ice0}, \tag{10}$$

which indicates that the incorporated dark materials from below become equal to the initial amount of ice. The analysis of the dark material yields the same result. The factor of $1 - f_0$ increases the amount of ice that must sublime. For instance, if $f_0 = 0.5$, then the final $d\phi$ must be 1.0 before all the ice is lost from the turn–over layer. Higher values of f_0 result in comparatively higher values of $d\phi$. The turn–over process continues over 4 Gyr such that the turn–over layer is always well mixed down to a constant depth d.

In our model, we consider that the icy sublimation would occur in this surface very thin layer which is characterized by the mixing (gardening) scales and that the sublimating layer incorporates the unturned-over material with an ice fraction of f_0 from below almost simultaneously with the sublimation. Thus we assume that the dark material cap would not form and the icy sublimation would continue. In this viewpoint, our model corresponds to the simplified version of the moving boundary problem (Crank, 1987) assuming that only the surface thin layer where the sublimation occurs is considered and that the formation and existence of the dark material cap is not considered. The moving boundary (i.e., Iapetus' surface) is implicitly considered by calculating the volume of the sublimated ice based on the albedo and the temperature in each time.

Based on the estimates by Neukum et al. (2006) and Schumedemann et al. (2008), impact cratering rate on the Iapetus' surface is approximately 0.06 times smaller than that on the terrestrial Moon: thus, the crater size-frequency distribution on the ancient (aged approximately 4.0 Gyr) Iapetus' surface is similar to that on the Moon's surface that is aged 3.3–3.4 Gyr. From the analogy regarding the depth scale of Lunar regolith, which is a few meters around this age (Hiesinger and Head, 2006), we consider the depth scale of the turn–over layer on Iapetus to be from 0.01 to 1.0 m (Heiken et al., 1991).

In this study, we assume the initial albedo distribution on Iapetus to be due to the exogenic dark materials deposited on the sur-

face. That is, the albedo at the apex is lowest and concentrically increases in a sinusoidal pattern. This situation simulates the existence of the dark material around the Iapetus' orbit billions of years ago when the synchronously rotating Iapetus swept the material. The ratio of the deposited materials gradually decreases with the distance from the apex. Fig. 6 is a typical example of the initial albedo distribution with a minimum albedo of 0.1 at the apex and maximum of 0.7 at the antapex. The model includes the periodic change of the Iapetus' obliquity with a 3000–year cycle and the eccentricity of the Saturn's orbit.

4 Results

This study is not aimed to find a definitive value for relevant material and structural properties, but is rather an exploratory investigation of the effects of ice sublimation on Iapetus and the long-time change of the albedo distribution by using a set of typical parameter values.

Fig. 7 shows the maximum surface temperature map based on the albedo distribution given in Fig. 6. This map represents that the highest temperature, approximately 127.5 K, is at and around the apex depending on the season and a higher temperature region elongates in the direction of the equator. This indicates that the change of solar altitude has a greater effect on the latitudinal difference of the surface temperature than on the longitudinal one.

Fig. 8 shows that the temporal changes of the surface albedo at the equator with various initial albedo values. The adopted parameters are described in Table 2. When the initial albedo is higher than ~ 0.5, ice hardly sublimes and the albedo changes slightly during 4.0 Gyr. On the other hand, when the albedo decreases to ~ 0.4, it decreases to zero over geologic time (precisely 0.01, which is the albedo of pure dark material). This indicates that the decreasing albedo causes an increase in the temperature,

and then ice sublimation accelerates resulting in further decreases in the albedo. This positive feedback process induces a rapidly changing albedo (Giese et al., 2008). In other words, once the surface experiences the feedback process, the surface albedo would be extremely low and cannot maintain an intermediate value. This trend is responsible for the clarity of the edge in a global view between the dark and bright regions.

The latitudinal difference of the long-time change of the albedo is shown in Fig. 9. In latitudes higher than 50 degrees, ice hardly sublimes and the albedo is almost constant with time, whereas at latitudes lower than ~ 45 degrees, ice sublimes effectively and the albedo decreases to the minimum of 0.01 for 4.0 Gyr. Note that even if the initial albedo and/or latitude are/is slightly different, the resultant albedos can differ significantly after billions of years.

Fig. 10 shows the long–time change of the albedo distribution. Initially, the dark materials were assumed to be accumulated in a concentric pattern around the apex, as shown in Fig. 6. After 4.0 Gyr, the resultant surface albedo has mainly three notable points. First, the albedo in the leading hemisphere has significantly decreased to approach the minimum value. Second, the dark region has been elongated along the equator. Third, the edge of the dark region has become clear. On the basis of the above results, we found that the resultant distribution of the surface albedo agrees very well with the current state. Therefore, it can be concluded that sublimation of ice expands the region of low albedo on Iapetus. Although both the external and endogenic hypotheses of the albedo dichotomy do not agree with all of these characteristics, the sublimation of the surface ice is a critical factor for determining the characteristics of the current dichotomy. These characteristics of the albedo distribution are determined mainly by two factors. The first factor is solar elevation. Even if the pristine dark materials are concentrically distributed around the apex, the temperature distribution elongates along the equator because of the large difference of the solar elevation angle among the latitudes. Thus, the resultant distribution of the dark region

is elliptical. The second factor is the albedo feedback process. As shown in Fig. 8, the final albedo will differ significantly after billions of years even if the initial difference of the albedo is small (For example, the initial values of 0.45 and 0.5 will be changed to 0.01 and 0.46 after 4.0 Gyr, respectively, as shown in Fig. 8). This sensitivity causes the clear edge of the dark region.

Moreover, calculations with various initial albedo values, which are distributed in the same pattern as Fig. 6, are performed and will apparently result in a different state after 4.0 Gyr. From these results, we found that the initial albedo distribution set to a minimum value of 0.2 at the apex and a maximum value of 0.6 at the antapex provide the best fit with the current extent of the dark region on Iapetus (Fig. 11 a). When the initial albedo is globally lower, the resultant albedo after 4 Gyr shows that the area of the dark region, where the albedo feedback occurs, becomes wider in the longitudinal direction (Fig. 11 b) On the other hand, when the albedo is globally higher (a minimum value of 0.4 at the apex and a maximum value of 0.8 at the antapex), as shown in Fig. 12, the dark region that experiences the albedo feedback (Fig. 6) is considerably restricted around the apex over 4.0 Gyr. This result does not agree with the current shape of the dark region.

We particularly noted that the ice sublimation and the subsequent darkening process have an effect on the current distribution of the dark material and the characteristics of the albedo dichotomy, respectively. The ice sublimation causes the elongation along the equator and the darkening process leads to the clarity of the edge of the dark region. However, the different extents of the region affected by the ice sublimation depend on the initial albedo value. Therefore investigation of the pristine distribution of the dark material is required to clarify the origin of the albedo dichotomy. Considering the icy sublimation effects, the current albedo distribution can be reconstructed from the sinusoidal albedo distribution, suggesting the apex-antapex cratering asymmetry as a candidate for the origin of the albedo dichotomy.

The total amount of the dark material and its distribution are important to clarify the origin of the dark material and the albedo dichotomy. Comparing the observed and calculated longitudinal extents of the dark region, we estimated the depth of the turn–over layer d where the darkening process proceeded for 4 Gyr (Fig. 13). As a result, the depth is 10 – 20 cm for the emissivity of 0.95 and 30 – 50 cm for the emissivity of 0.90 in order to form the observed extent of the dark region. This range of the depth is well consistent with the evaluation of decimeter thickness from the Cassini radar observations (Black et al., 2005; Ostro et al., 2006). In additon, the turn–over depth scale can be estimated by using analogy with the depth scale of Lunar regolith which is a few meters on the area having an age of 3.3–3.4 Gyr (Hiesinger and Head, 2006) as we discussed before. Because impact cratering rate on Iapetus is apploximately 0.06 times smaller than that on the terrestrial Moon (Neukum et al., 2006; Schumedemann et al., 2008), the crater size–frequency distribution on Iapetus' old surface that is aged about 4.0 Gyr is nearly equivalent to that on the Moon's surface that is aged about 3.3–3.4 Gyr. Therefore we consider the scale of turn–over depth on Iapetus to be from 0.01 to 1.0 m (Heiken et al., 1991).

5 Discussions

There are many simplified assumptions and uncertainties in physical parameters of the dark material in this study. In this section, we would like to explain the dependency of the material parameters on the albedo variation. The typical parameters and their values used in this study (shown in Fig. 7–12) are the albedo of the dark material $A_{dark} = 0.01$, the albedo of the pure H_2O ice $A_{ice} = 1.0$, the emissivity $\varepsilon = 0.9$, and the turn–over depth $d = 1.0$ m (listed in Table 2).

Fig. 14 a shows the result when A_{dark} is changed from 0.01 to 0.04, which corresponds to the current hemispheric albedo of the

leading side. This is the maximum value that can be considered for the albedo of the dark material. The result using $A_{ice} = 0.6$, which is changed from 1.0 in Fig. 11 a, is shown in Fig. 14 b. Both these results show only slightly smaller extent of the dark region than Fig. 11 a, and thus the difference of A_{dark} and A_{ice} have little effect on a long–time variation of albedo distribution.

For the emissivity, we used values between 0.70 and 0.95 because there are no substantial criteria to exactly determine a value. Although the value of 0.95 has been used in Palmer and Brown (2008) which focused on the surface stability of carbon dioxide on Iapetus, Spencer and Denk (2010) adopted the value of 1.0 for the albedo change on Iapetus, and Spencer (1987) which discussed the effect of ice sublimation on Galilean satellites also used the value of 1.0. The lower value of the emissivity facilitates an increase in the surface temperature and results in a significant enlargement of the dark region (Fig. 14 c).

If the turn–over depth d is smaller, the dark region after 4.0 Gyr will be wider (Fig. 14 d) because the depth d relates to the volume of mixtures of pure bright ice and dark material. Thus, the volume fraction of the dark material in the mixture progresses rapidly with ice sublimation for small values of d.

Furthermore, due to the Saturn's eccentricity, the distance to the Sun will change from 9.05 to 10.1 AU. This difference changes the solar flux and temperature over the course of an entire orbit. For examples, the peak temperature on Iapetus changes between 125.7 K (aphelion) and 133.1 K (perihelion) for the albedo of 0.04 and $\varepsilon = 0.90$, and thus the ice sublimation rate is in the range from 4.1×10^{-12} to $5.7\times10^{-11}\,\mathrm{kg/m^2\,s}$. The initial albedo that completely darkens in 4.0 Gyr differs by only a few percent among cases with orbital variation (~ 0.47, see Fig. 8) and without it (~ 0.45). The longitudinal extent of the dark region after 4 Gyr for the model without orbital variation will be about 10 degrees smaller than that in the case with orbital variation (Fig. 15).

This work is based on the fact that the huge dust ring exiets around the orbit of Phoebe (Verbiscer et al., 2009), supporting strongly the external hypothesis of the dark material. Although this work assumes that the dark material is intially deposited and following turn–over does not add the dark material on Iapetus, the time-varying effect of infall rate and gardening (i.e., initially, gardening and supplying the dark material is effective, but over time, it becomes a minor process that can be neglected) might be considered in a future work.

Although we do not consider recondensation of the sublimed ice in this study, it possibly contributes to the high albedo region at the higher latitudes on Iapetus, where the temperature is sufficiently low for recondensation (Spencer and Denk, 2010).

Jovian icy moons Ganymede and Callisto have also low albedo, 0.25 and 0.31, respectively (Squyres, 1980), but they possibly should not have experienced the runaway sublimation unlike Iapetus. The ice on these moons and has a larger grain size because of higher temperature environment and following the sintering process of icy grains. The ice with large grain size tends to have a lower albedo even that a smaller amount of the dark materials is included in the ice. Also, Iapetus ' small gravity makes the sublimated ice travels long distance (or escape to the space), and finally global hemispheric dichotomy will be formed on only Iapetus. On the other hand, on Ganymede and Callisto the sublimated ice travels to shorter distance and albedo contrast will be formed locally because of their larger size and gravity. In addition, different environment to create an initial albedo distribution between Iapetus and Galilean moons need to be discussed carefully. Various aspects should be taken into account and this issue is worth investigating in a future work.

6 Summary

This study investigated the effect of ice sublimation on the distribution of the surface albedo on Iapetus. We can conclude the following:

- If seeded with enough dark material, sublimation of H_2O ice would drastically change the distribution of the surface albedo. Although material parameters have large uncertainty, the long-time effect of ice sublimation yielded results significantly different from the initial albedo state in all settings.
- By considering the effect of ice sublimation, the current characteristics of the albedo distribution can be expressed. The first characteristic is the elongation of the dark region along the equator. Because the solar elevation angle largely depends on the latitude, the temperature distribution elongates along the equator even if the initial albedo distribution was concentric. The second characteristic is the clarity of the edge between the dark and bright regions owing to the runaway feedback process of the surface albedo.
- The hypothesis of an eruptive origin from an equatorial ridge is not necessary to explain the origin of the albedo dichotomy. This endogenic hypothesis is based on the coincidence between the elongation of the dark region along the equator and the existence of the equatorial ridge. However, we showed that the elongated shape of the dark region can be explained by the initial albedo distribution that assumes the external hypothesis (i.e., the apex–antapex asymmetry) if ice sublimation is considered.
- We found the initial albedo distribution that explained the current state. The most suitable setting for the initial albedo state to reconstruct the current distribution is 0.2 at the apex and 0.6 at the antapex, having concentric and gradual variation.

Acknowledgments

The authors wish to thank three anonymous reviewers for constructive comments which greatly benefited the paper. We appreciate the help of Y. Yokota for calculation using SPICE toolkit. This work was supported by the Grant-in-Aid for Young Scientists (B), MEXT.

References

Ackerman, T. P., Toon, O. B., 1981. Absorption of visible radiation in atmosphere containing mixtures of absorbing and nonabsorbing particles. Applied Optics 20, 3661–3668.

Acton, C. H., 1996. Ancillary data services of NASA's Navigation and Ancillary Information Facility. Planetary and Space Sciences 44, 65–70.

Andreas, E. L., 2007. New estimates for the sublimation rate for ice on the Moon. Icarus 186, 24–30.

Bell, J. F., Cruikshank, D. P., Gaffey, M. J., 1985. The composition and origin of the Iapetus dark material. Icarus 61, 192–207.

Black, G. J., Campbell, D. B., Carter, L. M., Ostro, S. J., 2005. Radar Detection of Iapetus. Science 304, 553.

Buratti, B. J., Mosher, J. A., 1995. The dark side of Iapetus: Additional evidence for an exogenous origin. Icarus 115, 219–227.

Buratti, B. J., Hicks, M. D., Davies, A., 2005. Spectrophotometry of the small satellites of Saturn and their relationship to Iapetus, Phoebe, and Hyperion. Icarus 175, 490–495.

Buratti, B. J., Soderlund, K., Bauer, J., Mosher, J. A., Hicks, M. D., Simonelli, D. P., Jaumann, R., Clark, R. N., Brown, R. H., Cruikshank, D. P., Momary, T., 2008. Infrared (0.83-5.1μ m) photometry of Phoebe from the Cassini Visual Infrared Mapping Spectrometer. Icarus 193, 309–322.

Castillo-Rogez, J. C., Matson, D. L., Sotin, C., Johnson, T. V.,

Lunine, J. I., Thomas, P. C., 2007. Iapetus' geophysics: Rotation rate, shape, and equatorial ridge. Icarus 190, 179–202.

Crank, J, 1987. Moving-boundary problems: formulation. In Free and Moving Boundary Problems. Oxford Science Publications, pp. 1–29.

Cruikshank, D. P., Bell, J. F., Gaffey, M. J., Brown, R. H., Howell, R., Beerman, C., Rognstad, M., 1983. The dark side of Iapetus. Icarus 53, 90–104.

Cruikshank, D. P., Wegryn. E., Ore, C. M., Brown, R. H., Bibring, J.-P., Bu-ratti, B. J., Clark, R. N., McCord, T. B., Nicholson, P. D., Pendleton, Y. J., Owen, T. C., Filacchione, G., Coradini, A., Cerroni, P., Capaccioni, F., Jaumann, R., Nelson, R. M., Baines, K. H., Sotin, C., Bellucci, G., Combes, M., Langevin, Y., Sicardy, B., Matson, D. L., Formisano, V., Drossart, P., Mennella, V., 2008, Hydrocarbons on Saturn's satellites Iapetus and Phoebe. Icarus 193, 334–343.

Cuzzi, J. N., Estrada, P. R., 1998, Compositional Evolution of Saturn's Rings Due to Meteoroid Bombardment. Icarus 132, 1–35.

Denk, T., Neukum, G., 2000. Iapetus (2): Dark-Side Origin. Lunar Planet. Sci. Abst. 31, 1660.

Denk, T., Neukum, G., Roatsch, T., McEwen, A. S., Turtle, E. P., Thomas, P. C., Helfenstein, P., Wagner, R. J., Porco, C. C., Perry, J. E., Giese, B., Johnson, T. V., Veverka, J., and the Cassini ISS Team, 2005. First imaging results from the Iapetus b/c flyby of the Cassini Spacecraft. Lunar Planet. Sci. Abst. 36, 2268.

Dozier, J., Warren, S. G., 1982, Effect of Viewing Angle on the Infrared Brightness Temperature of Snow. Water Resources Research 18, 1424–1434.

Estermann, I., 1955. Gases at low densities. In: Rossini, F. D. (Ed.), Thermodynamics and Physics of Matter. Princeton Univ. Press, Princeton, pp. 736–776.

Filacchione, G., Capaccioni, F., McCord, T. B., Coradini, A., Cerroni, P., Bellucci, G., Tosi, F., Aversa, E. D ', Formisano, V., Brown, R. H., Baines, K. H., Bibring, J. P., Buratti, B. J.,

Clark, R. N., Combes, M., Cruikshank, D. P., Drossart, P., Jaumann, R., Langevin, Y., Matson, D. L., Mennella, V., Nelson, R. M., Nicholson, P. D., Sicardy, B., Sotin, C., Hansen, G., Hibbitts, K., Showalter, M., Newman, S., 2007. Saturn's icy satellites investigated by Cassini-VIMS I. Full-disk properties: 350-5100 nm reflectance spectra and phase curves. Icarus 186, 259–290.

Gault, D. E. Horz, F., Brownlee, D. E., Hartung, J .B., 1974. Mixing of the lunar regolith. Proc. of the 5th. Lunar Conference 3, 2365–2386.

Giese, B., Denk, T., Neukum, G., Roatscha, T., Helfenstein, P., Thomas, P. C., Turtle, E. P., McEwen, A., Porco, C. C., 2008. The topography of Iapetus' leading side. Icarus 193, 359–371.

Heiken, G. H., Vaniman, D., French, B. M., 1991. Lunar Sourcebook, a user's guide to the Moon. NewYork: Cambridge University Press. 736 p.

Hendrix, A. R. Hansen, C. J., 2008. The albedo dichotomy of Iapetus measured at UV wavelengths. Icarus 193, 344–351.

Hiesinger, H., Head, J. W. III, 2006. New views of Lunar geoscience: An introduction and overview, in New Views of the Moon. Mineralogical Society of America, Geochemical Society. 1–81.

Jarvis, K. S., Viras, F., Larson, S. M., Gaffey, M. J., 2000. Are Hyperion and Phoebe Linked to Iapetus? Icarus 146, 125–132.

Jaumann, R., Clark, R. N., Nimmo, F., Hendrix, A. R., Buratti, B. J., Denk, T., Moore, J. M., Schenk, P. M., Ostro, S. J., Srama, R., 2009. Icy Satellites: Geological Evolution and Surface Processes. In: Dougherty, M. K., Esposito, L. W., Krimigis, S. M. (Ed.) Saturn. Springer, pp. 637–681.

Lebofsky, L. A., Feierberg, M. A., Tokunaga, A. T., 1982. Infrared observations of the dark side of Iapetus. Icarus 49, 382–386.

Murphy, D. M., Koop, T., 2005. Review of the vapour pressures of ice and super-cooled water for atmospheric applications. Q. J. R. Meteorol. Soc. 131, 1539–1565.

Neukum, G., Wagner, R., Wolf, U., Denk, T., 2006. The Cratering Record and Cratering Chronologies of the Saturnian Satellites

and the Origin of Impactors: Results from Cassini ISS Data. Abstract for European Planetary Science Congress.

Ostro, S. J., West, R. D., Janssen, M. A., Lorenz, R. D., Zebker, H. A., Black, G. J., Lunine, J. I., Wye, L. C., Lopes, R. M., Wall, S. D., Elachi, C., Roth, L., Hensley, S., Kelleher, K., Hamilton, G. A., Gim, Y., Anderson, Y. Z., Boehmer, R. A., Johnson, W. T. K., and the Cassini RADAR Team, 2006. Cassini RADAR observations of Enceladus, Tethys, Dione, Rhea, Iapetus, Hyperion, and Phoebe. Icarus 183, 479–490.

Owen, T. C., Cruikshank, D. P., Dalle Ore, C. M., Geballe, T. R., Roush, T. L., de Bergh, C., Meier, R., Pendleton, Y. J., Khare, B. N., 2001. Decoding the Domino: The Dark Side of Iapetus. Icarus 149, 160–172.

Palmer, E. E. and Brown, R. H., 2008. The stability and transport of carbon dioxide on Iapetus. Icarus 195, 434–446.

Schmedemann, N., Neukum, G., Denk, T., Wagner, R., 2008. Stratigraphy and Surface Ages on Iapetus and Other Saturnian Satellites. Abstract for Lunar and Planetary Science Conference, 2070.

Sinclair, A. T., 1974. A theory of the motion of Iapetus. MNRAS 169, 591–605.

Smith, B. A., Soderblom, L., Batson, R. M., Bridges, P. M., Inge, J. L., Masursky, H., Shoemaker, E., Beebe, R. F., Boyce, J., Briggs, G., Bunker, A., Collins, S. A., Hansen, C., Johnson, T. V., Mitchell, J. L., Terrile, R. J., Cook, A. F., Cuzzi, J. N., Pollack, J. B., Danielson, G. E., Ingersoll, A. P., Davies, M. E., Hunt, G. E., Morrison, D., Owen, T., Sagan, C., Veverka, J., Strom, R., Suomi, V. E., 1982. A new look at the Saturn system - The Voyager 2 images. Science 215, 504–537.

Spencer, J. R., 1987. Thermal Segregation of Water Ice on the Galilean Satellites. Icarus 69, 297–313.

Spencer, J. R., Denk, T., 2010. Formation of Iapetus' Extreme Albedo Dichotomy by Exogenically Triggered Thermal Ice Migration. Science 327, 432–435.

Squyres, S. W., 1980. Surface temperatures and retention of H2O frost on Ganymede and Callisto. Icarus 44, 502–510.

Squyres, S. W., Sagan, C., 1983. Albedo asymmetry of Iapetus. Nature 303, 782–785.

Soter, S., Paper presented at the IAU Colloquium 28, Cornell University, Ithaca, NY, 18 to 21 August 1974.

Thomas, P., Veverka, J., 1985. Hyperion: Analysis of Voyager Observations. Icarus 64, 414–424.

Thomas, P. C., Burns, J. A., Helfenstein, P., Squyres, S., Veverka, J., Porco, C., Turtle, E. P., McEwen, A., Denke, T., Giese, B., Roatsch, T., Johnson, T. V., Jacobson, R. A., 2007. Shapes of the saturnian icy satellites and their significance. Icarus 190, 573–584.

Veeder, G. J., Matson, D. L., 1980, The relative reflectance of Iapetus at 1.6 and 2.2 microns. astron. Journal 85, 969–972.

Verbiscer, A. J., Skrutskie, M. F., Hamilton, D. P., 2009. Saturn' largest ring. nature 461, 1098–1100.

Vilas, F., Larson, S. M., Stockstill, K. R., Gaffey, M. J., 1996. Unraveling the Zebra: Clues to the Iapetus Dark Material Composition. Icarus 124, 262–267.

Ward, W. R., 1981. Orbital inclination of Iapetus and the rotation of the Laplacian plane. Icarus 46, 97–107.

Yoder, C. F., 1995. Astrometric and geodetic properties of Earth and the Solar System. In: Ahrens, T.J. (Ed.), A Handbook of Physical Constants: Global Earth Physics. AGU Reference Shelf Series, vol. 1. ISBN 0-87590-851-9, pp. 1–31.

Zahnle, K., Dones, L., Levison, H. F., 1998. Cratering rates on the Galilean satellites. Icarus 136, 202–222.

Table 1
Properties of Iapetus.

Properties	Values	References
Mean radius (km)	735.6 ± 3.0	Thomas et al. (2007)
Mean density (kg/m^3)	1083 ± 13	Thomas et al. (2007)
Orbital semimajor axis (km)	3.5613 ± 10^6	Yoder (1995)
Orbital eccentricity	0.0283	Yoder (1995)
Orbital obliquity (degrees in respect to Laplace plane)	7.52	Yoder (1995)
Orbital period (Earth days)	79.330183	Yoder (1995)

Table 2
Parameter sets for the calculation of albedo change.

Figure number	albedo of the dark material (A_{dark})	albedo of the pure H_2O ice (A_{ice})	initial albedo at the apex	initial albedo at the antapex	emissivity (ε)	depth (d) [m]
Fig. 7, 8, 9, 10	0.01	1.0	0.1	0.7	0.90	1.0
Fig. 11 (a)	0.01	1.0	0.2	0.6	0.90	1.0
Fig. 11 (b)	0.01	1.0	0.1	0.5	0.90	1.0
Fig. 12	0.01	1.0	0.4	0.8	0.90	1.0
Fig. 13	0.01	1.0	0.1	0.7	0.90, 0.95	0.01 – 1.0
Fig. 14 (a)	0.04	1.0	0.2	0.6	0.90	1.0
Fig. 14 (b)	0.01	0.6	0.2	0.6	0.90	1.0
Fig. 14 (c)	0.01	1.0	0.2	0.6	0.70	1.0
Fig. 14 (d)	0.01	1.0	0.2	0.6	0.90	0.1
Fig. 15	0.01	1.0	0.1	0.7	0.90	1.0

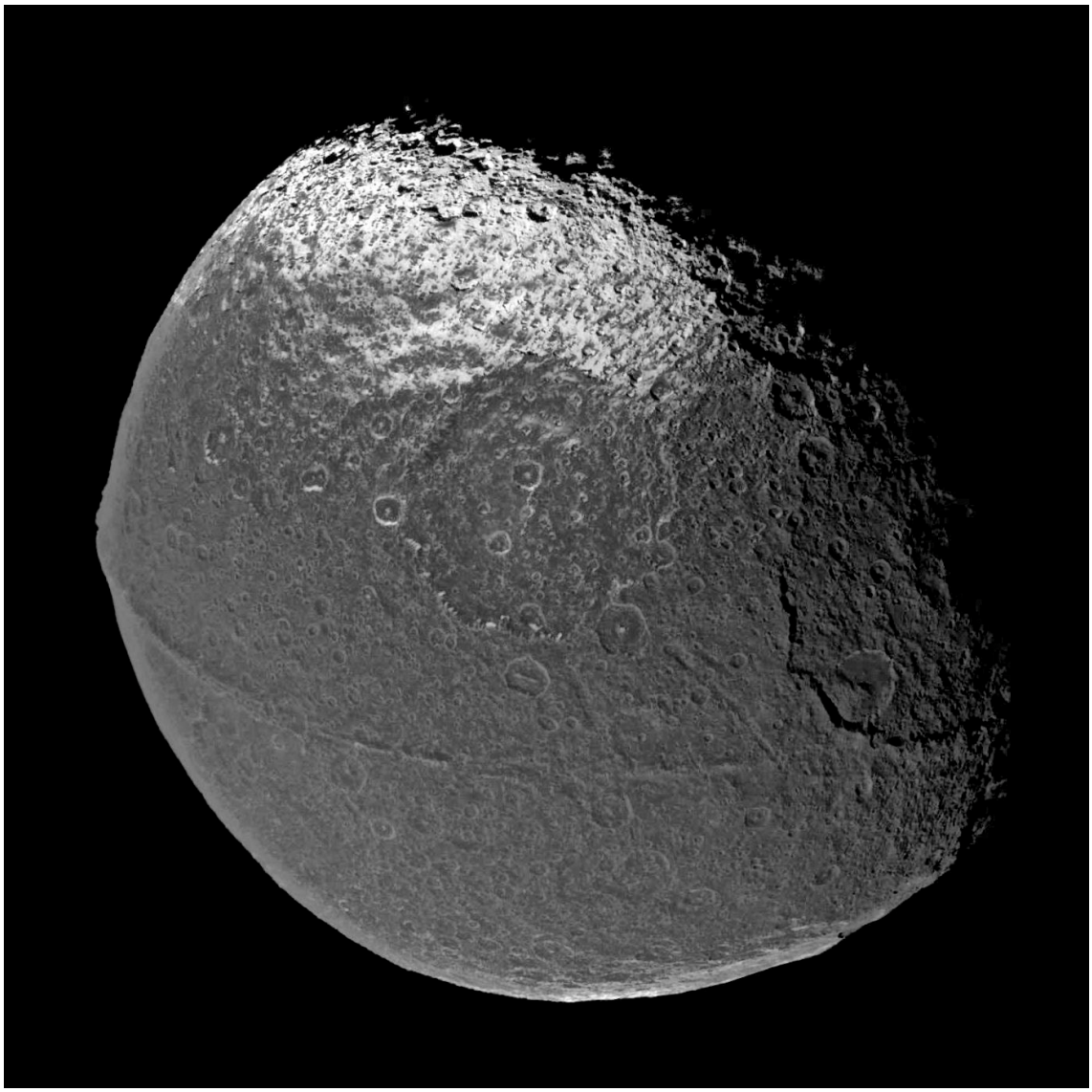

Fig. 1. Saturnian moon Iapetus, imaged by Cassini spacecraft at a distance of about 172,400 km (107,124 miles) from Iapetus (PIA06166: http://Saturn.jpl.nasa.gov/photos). The view is centered on Iapetus' equator (which coincides almost exactly with a topographic ridge) and on approximately 90° W (the location of the apex, center of the leading hemisphere).

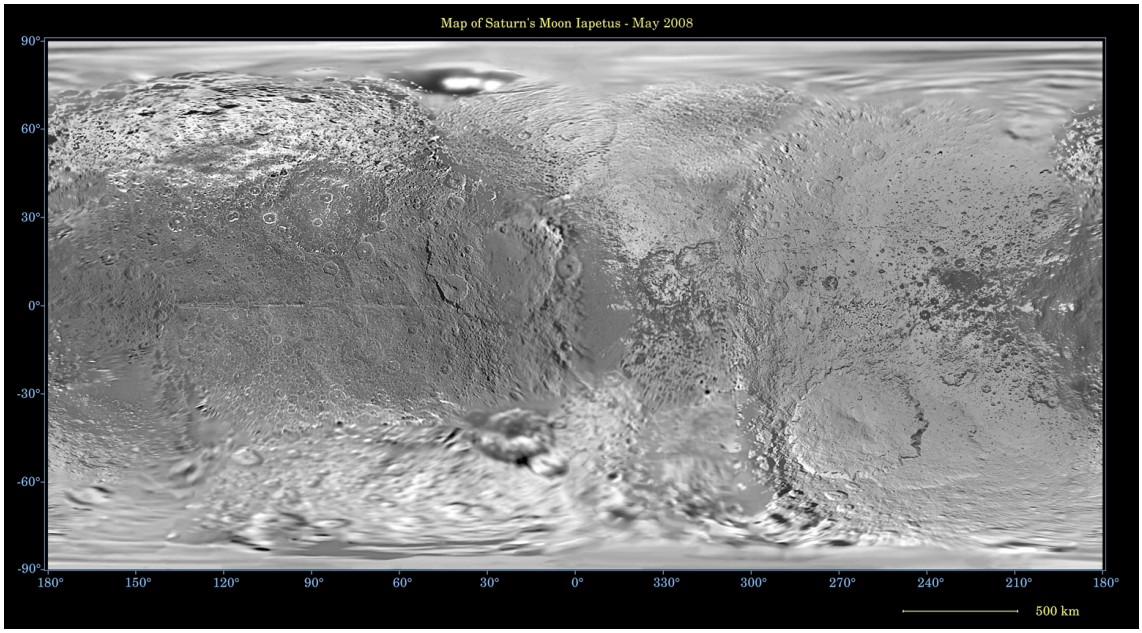

Fig. 2. Global digital map of Iapetus from data taken during Cassini spacecraft flybys, with Voyager images filling in the gaps in Cassini's coverage (PIA11116: http://Saturn.jpl.nasa.gov/photos). The dark materials are concentrated on the leading hemisphere (that faces forward in Iapetus' orbit, centered near 90° W longitude).

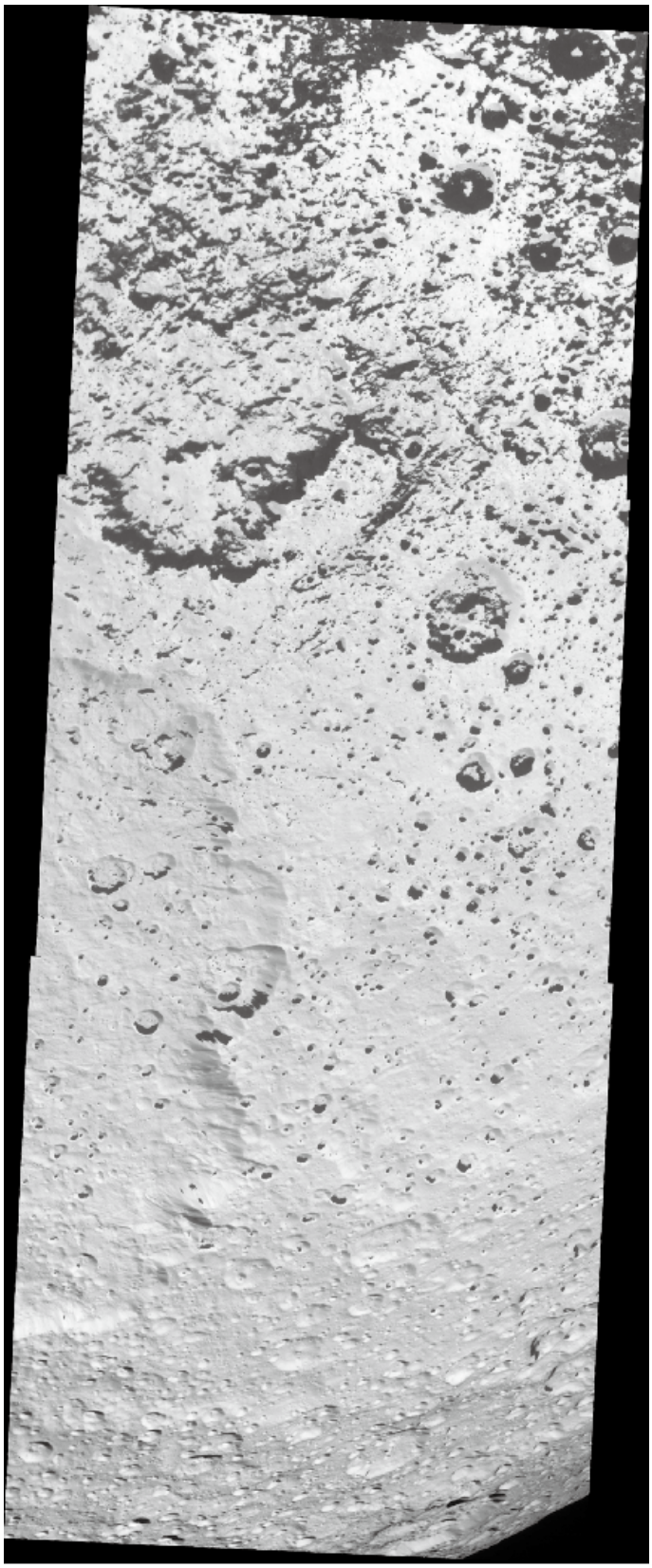

Fig. 3. Close-up image of Iapetus' southern trailing hemisphere (a part of the boundary region separating the dark leading and bright trailing hemispheres) obtained with the Cassini spacecraft. The dark area appears on the northern-facing walls and the floors of low and middle latitude craters (the equator is located above this image). Meanwhile higher-latitude craters (lower in the image) show no dark region on any side of wall or floor.

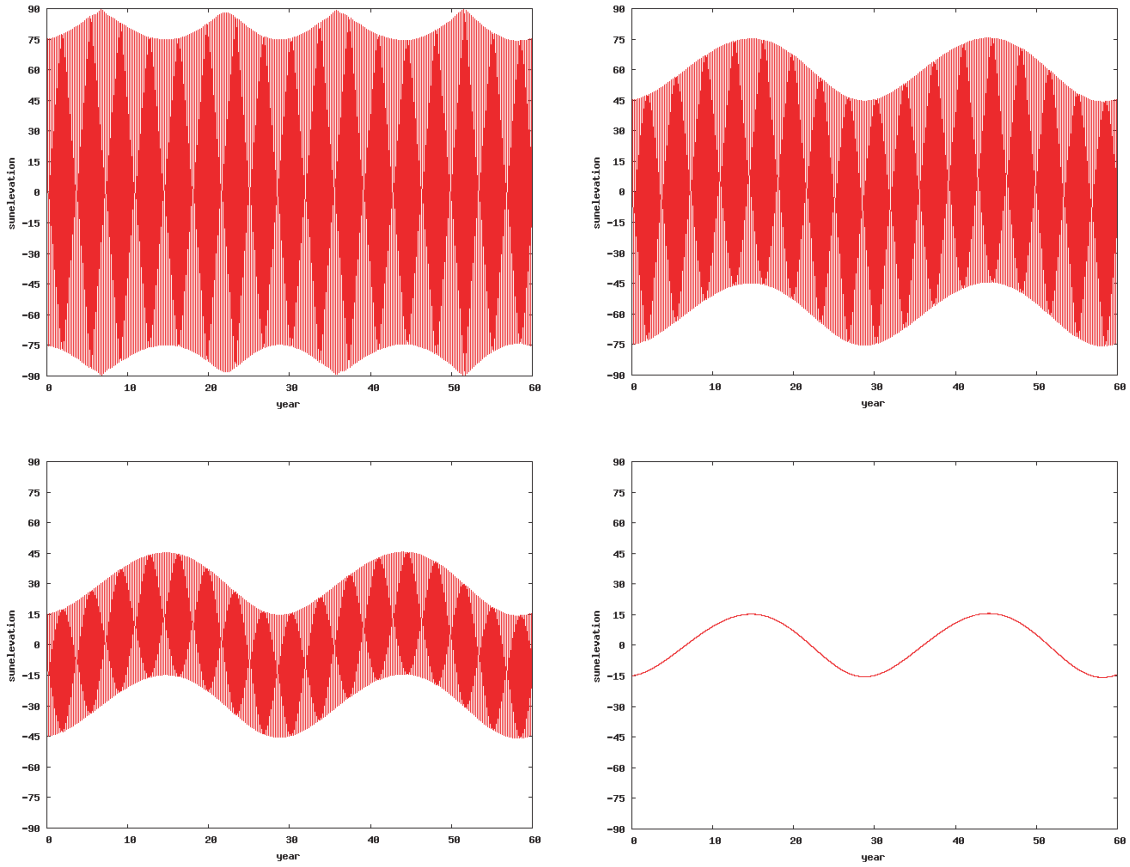

Fig. 4. Changes of solar altitude at Iapetus' surface for 60 Earth years (corresponds to about 2 Saturn years) using the SPICE toolkit provided by the Navigation and Ancillary Information Facility (NAIF)/JPL/NASA (Acton, 1996). The solar altitude is defined as degrees from the horizon (0° being horizon, +90° being zenith), and negative values of the solar altitude indicate that the area is in the nighttime. 0° (upper left), 30° (upper right), 60° (lower left), and 90° of latitude (lower right) are shown.

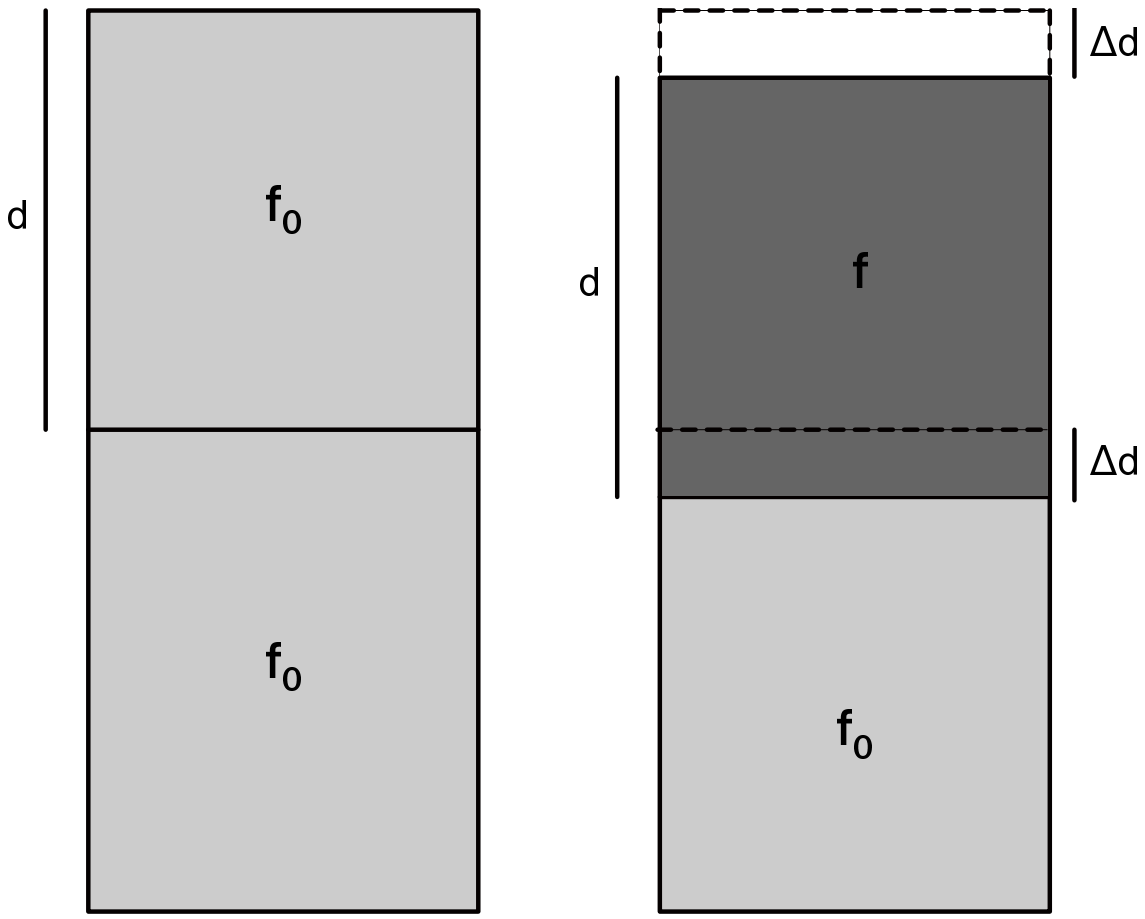

Fig. 5. Schematic view of the surface structural model for icy sublimation. d is the turn–over depth, Δd is the cumulative depth due to the icy sublimation, which is dV/S, f_0 is the initial fraction of ice, and f is the fraction in the turn–over layer. Initial state (left), and the state that ice sublimed after dt (right).

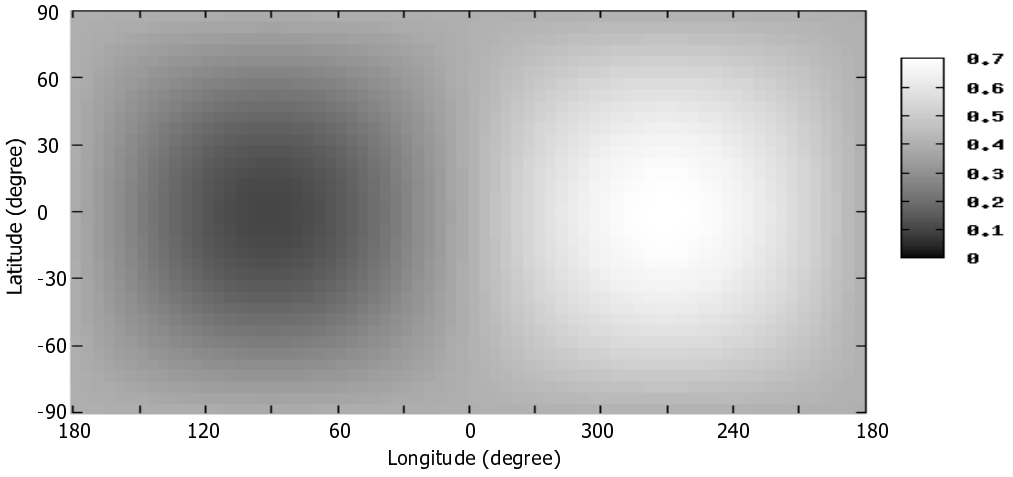

Fig. 6. Example of the initially gradual distribution of surface albedo. Albedos at the apex (90° longitude, 0° latitude) and antapex (270° longitude, 0° latitude) are assumed to be 0.1 and 0.7, respectively.

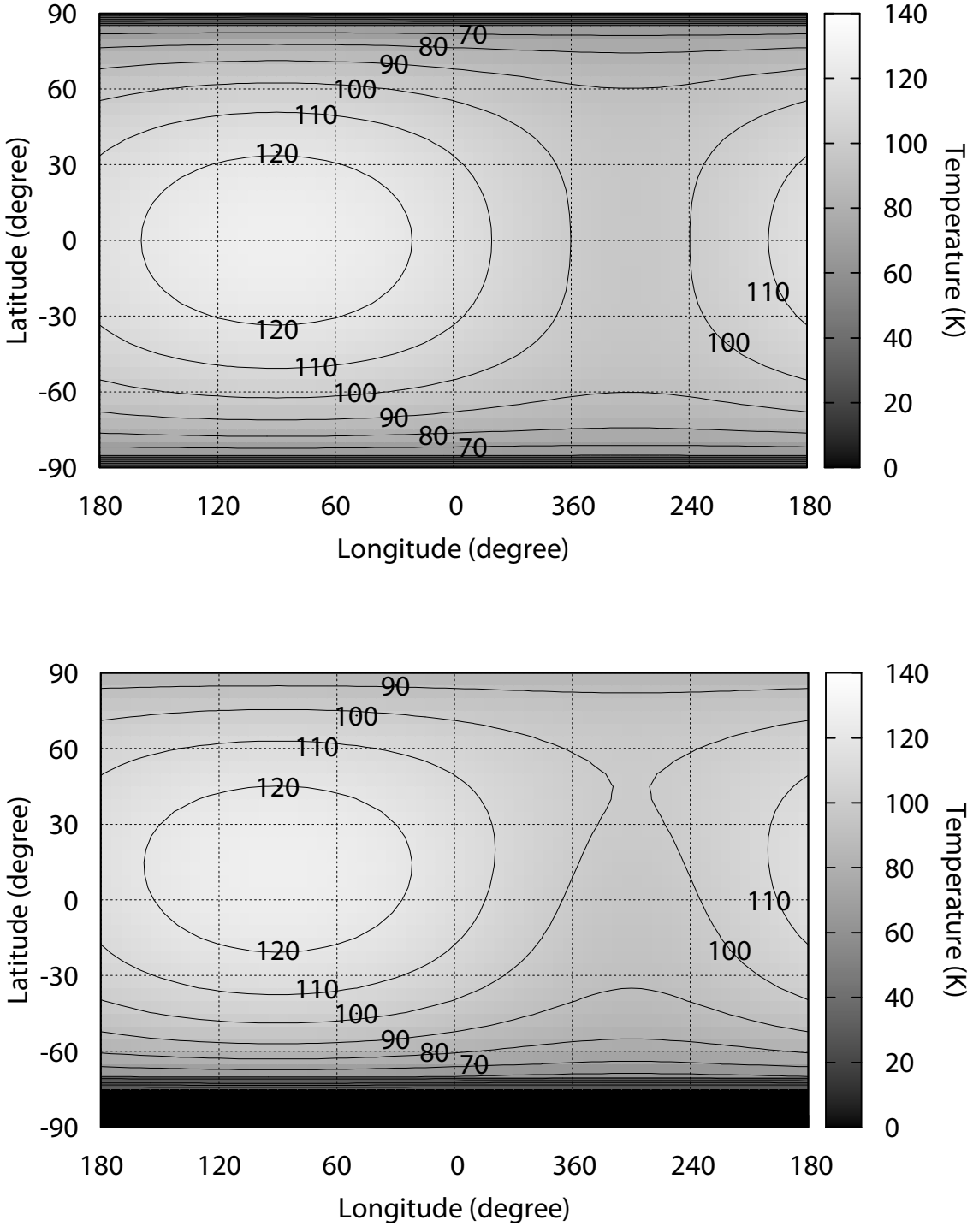

Fig. 7. Maximum surface temperature map, based on the albedo distribution given in Figure 6. Upper: On the equinox, the solar altitude at the equator is the highest. Lower: On the northern solstice, the solar altitude at the equator is 15.4°. We use the emissivity (ε) of 0.90.

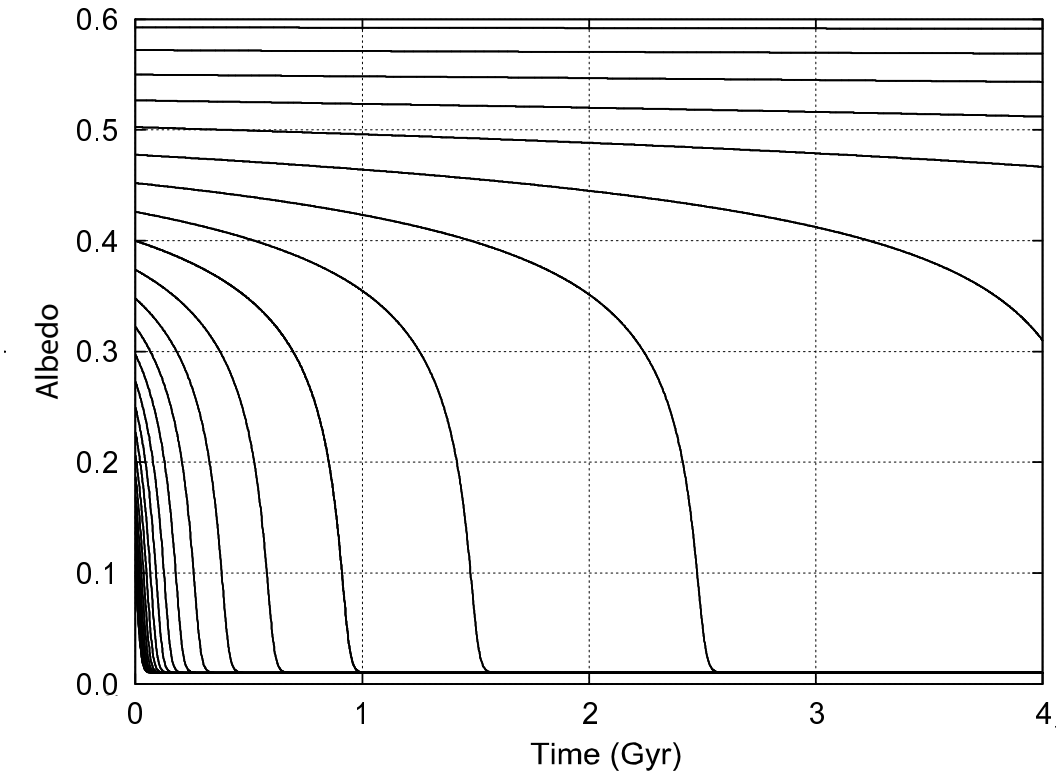

Fig. 8. Temporal changes of the surface albedo at the equator with various initial albedo values. When the initial value is 0.5 or higher, the albedo is almost constant over billions of years. On the other hand, when the initial value is 0.47 or lower, the albedo decreases to approach zero over geologic time.

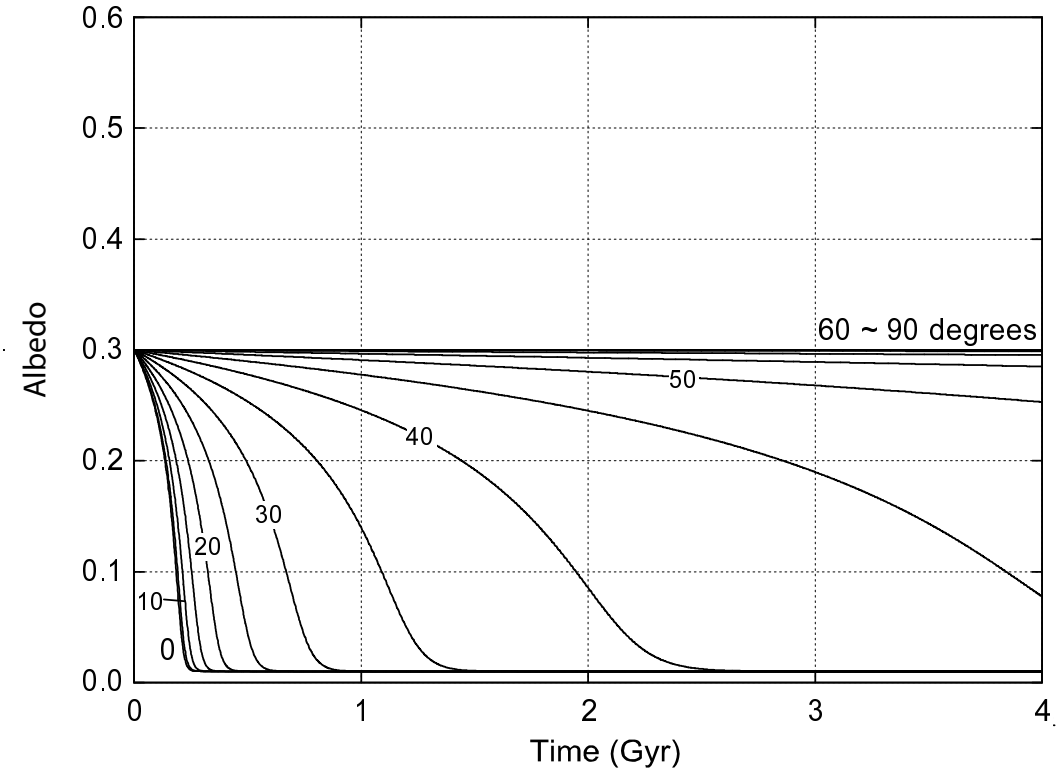

Fig. 9. Temporal changes of the surface albedo in various latitudinal zones for an initial albedo of 0.3. In latitudes higher than 50 degrees, the icy sublimation will hardly occur and the albedo will be almost constant with time. On the other hand, the albedo at latitudes of 45° or lower decreases to the minimum of 0.01 for 4.0 Gyr.

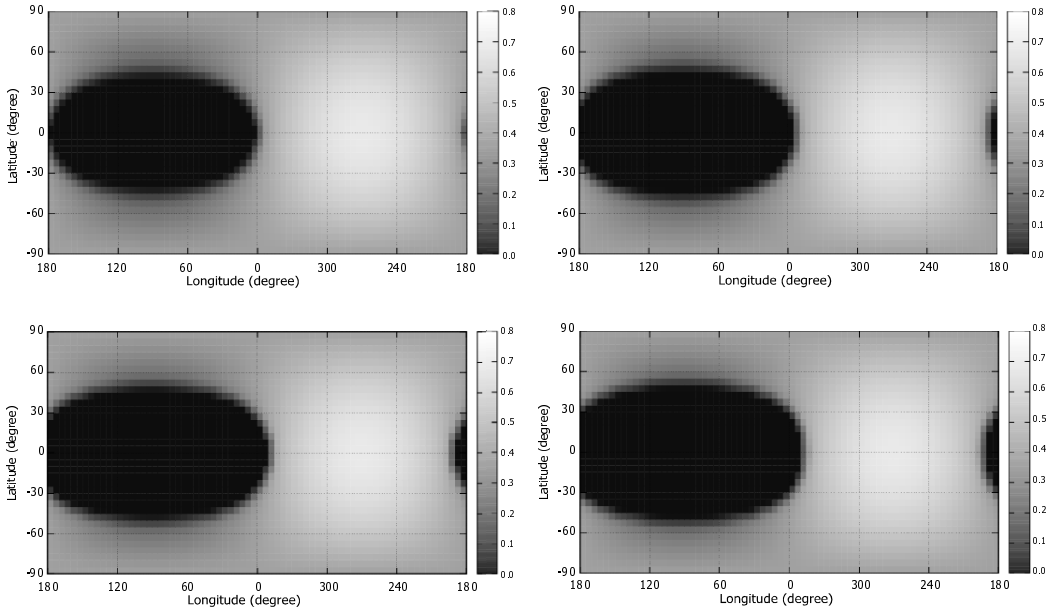

Fig. 10. Snapshots of the surface albedo distribution per 1 Gyr using the initial condition given by Fig. 6. The results are in 1.0 Gyr (upper left), 2.0 Gyr (upper right), 3.0 Gyr (lower left), and 4.0 Gyr (lower right), respectively.

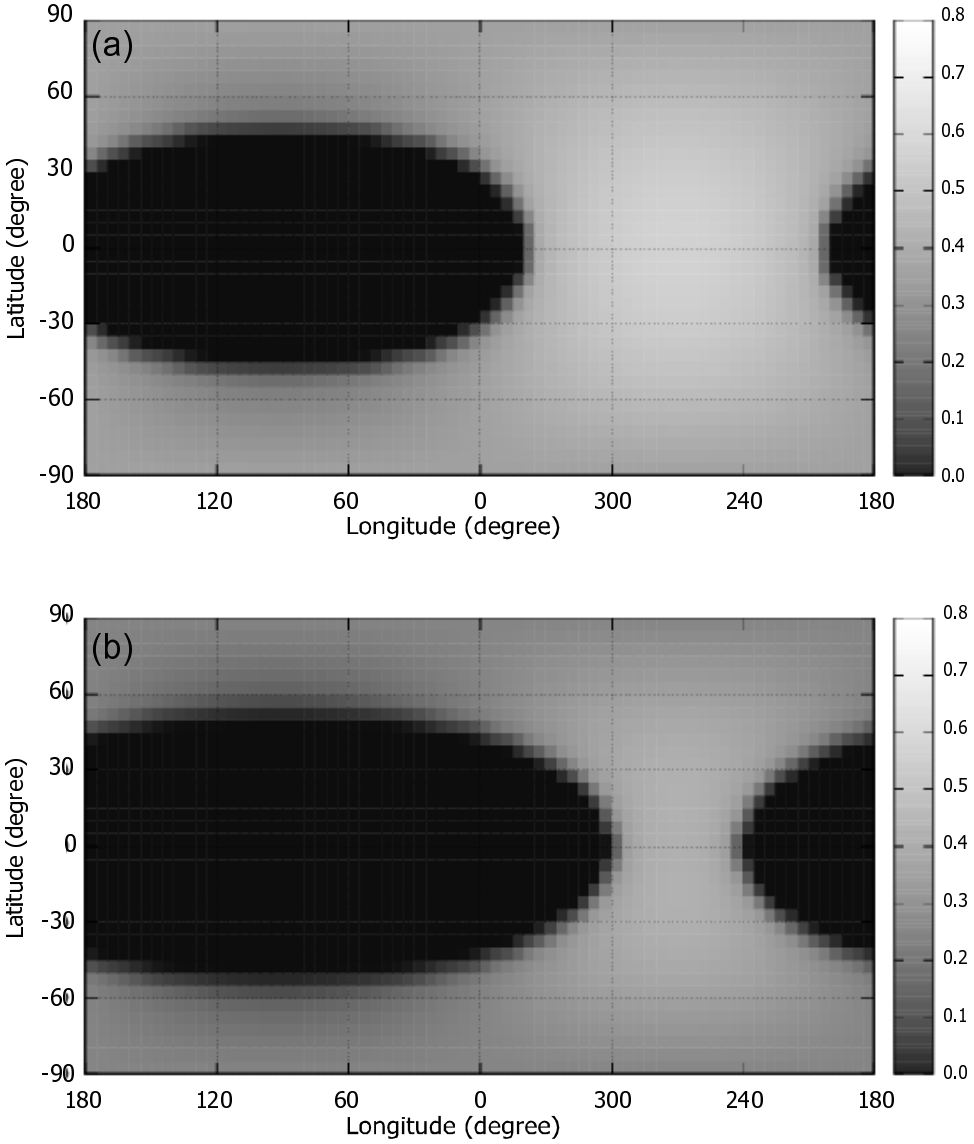

Fig. 11. (a) The albedo map after 4.0 Gyr with initial albedo distribution which is set to be 0.2 at the apex and 0.6 at the antapex. This distribution best fits the actual current distribution on Iapetus within various parameters used in this study. (b) Same map as above but with initial albedo distribution which is set to 0.1 at the apex and 0.5 at the antapex. The dark region is wider, which is not consistent with the actual current distribution.

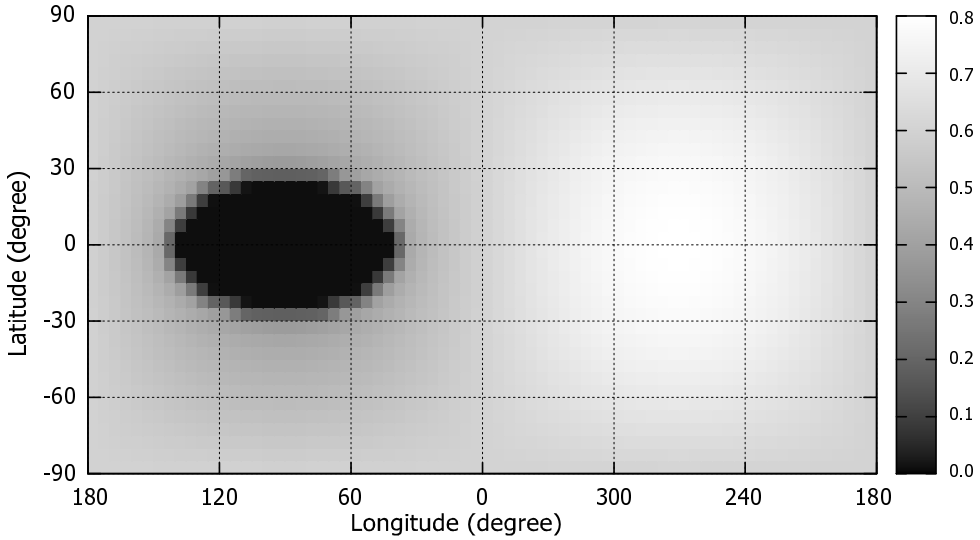

Fig. 12. The albedo map after 4.0 Gyr with initial albedo distribution having a value of 0.4 at the apex and 0.8 at the antapex. The dark region is extremely smaller compared with the actual current one and thus, this result appears to be inconsistent with the observation.

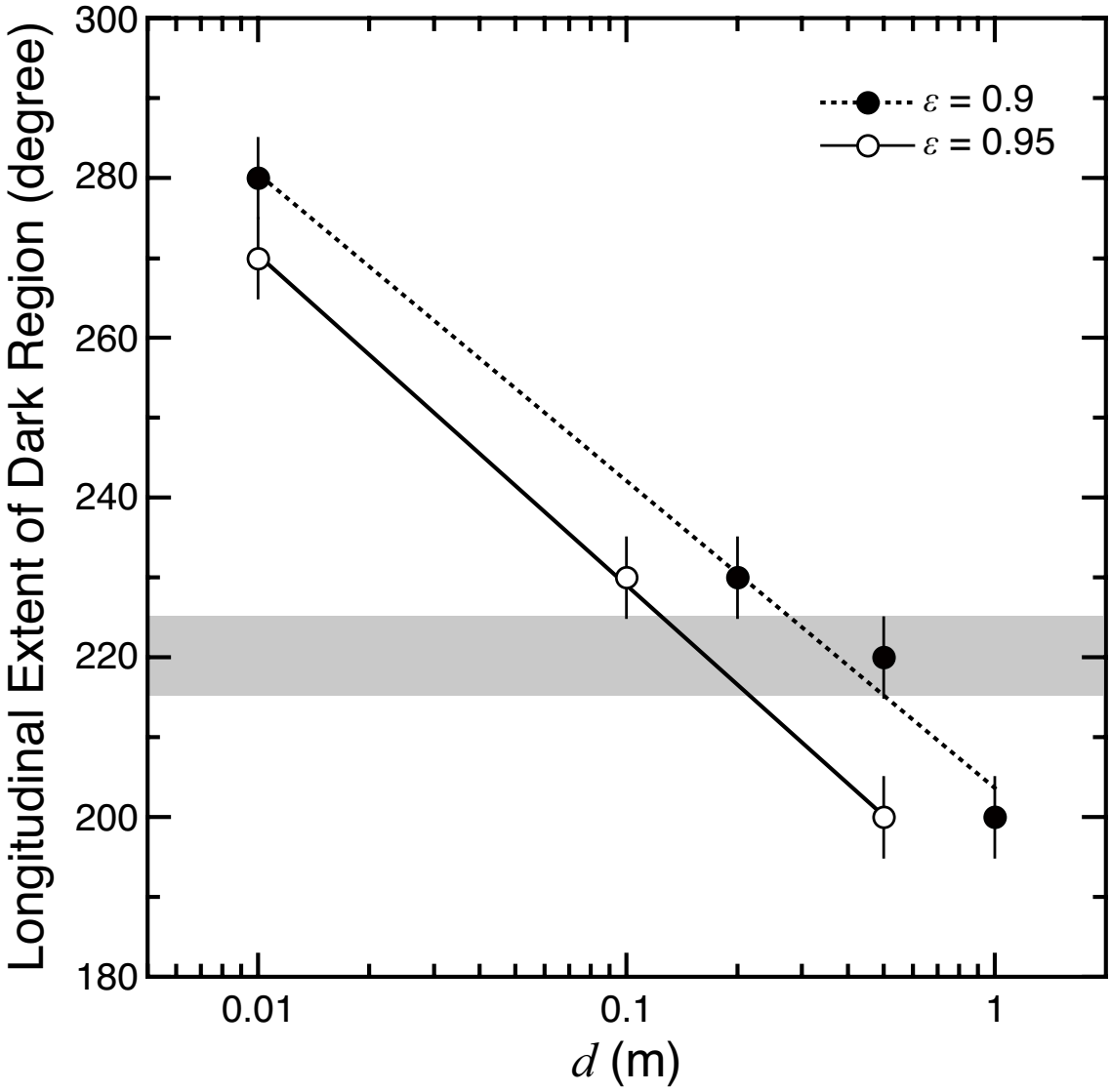

Fig. 13. Longitudinal extent of the dark region as a function of the turn–over depth d. For all plots, initial albedo is set to 0.1 at the apex and 0.7 at the antapex (see Fig. 6) with $A_{dark} = 0.01$ and $A_{ice} = 1.0$ (see Table 2). We defined the region with lower albedo than 0.1 as the dark region and evaluated its longitudinal width, and error bars are defined as a spatial resolution of our calculation (5 degrees). Hatched area indicates the longitudinal width of the dark Cassini Regio, which is measured from the global map of Iapetus (Fig. 2).

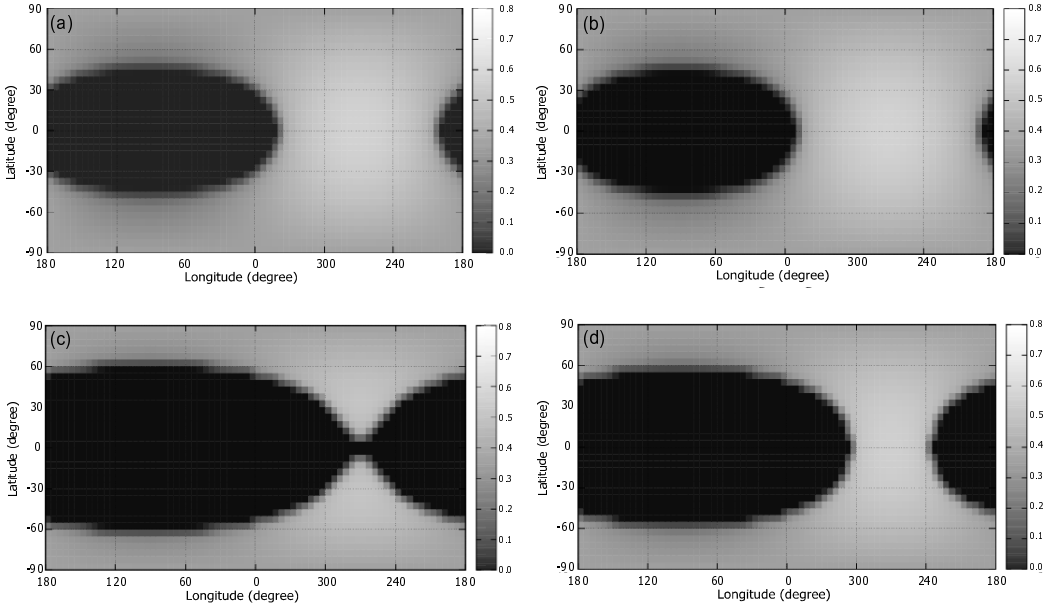

Fig. 14. Albedo maps after 4.0 Gyr in the case that some parameters were changed from those best–fitted case (Fig. 11 a). (a) Result for changing A_{dark} from 0.01 to 0.04, (b) A_{ice} from 1.0 to 0.6, (c) ε from 0.9 to 0.7, (d) d from 1.0 to 0.1. Parameter sets are described in Table 2.

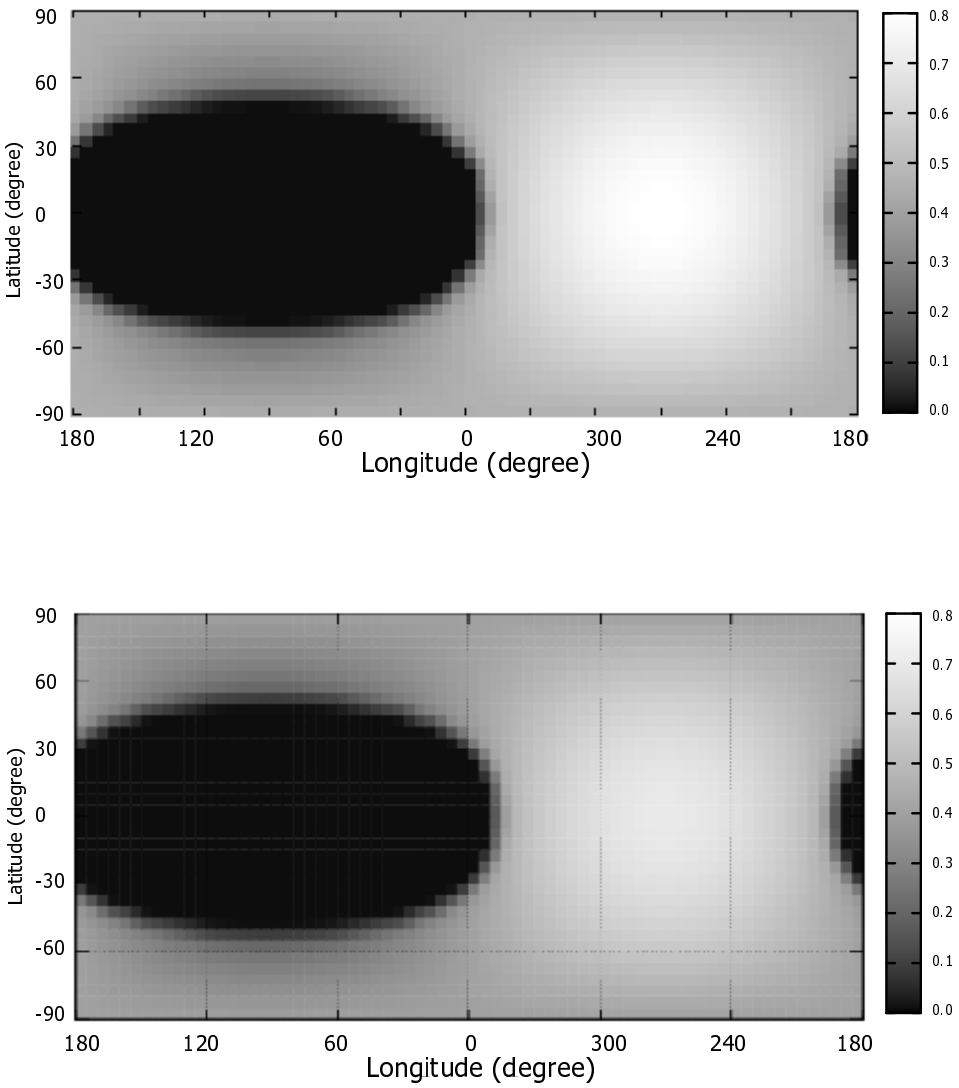

Fig. 15. Albedo map after 4 Gyr in calculation without orbital variation (upper) and with it (lower). This shows that longitudinal extent of the dark region in the case with orbital variation is about 10 degrees larger than that in the case without orbital variation.